




# Poly(vinylidene fluoride-trifluoroethylene)/cobalt ferrite composite films with a self-biased magnetoelectric effect for flexible AC magnetic sensors

Xuejian Mu<sup>1</sup>, Hao Zhang<sup>1</sup>, Chenyan Zhang<sup>1</sup>, Shuya Yang<sup>1</sup>, J. Xu<sup>1</sup>, Yicong Huang<sup>1</sup>, Jie Xu<sup>1,\*</sup> , Yongcheng Zhang<sup>1</sup>, Qiang Li<sup>1</sup>, Xia Wang<sup>1</sup>, Derang Cao<sup>1</sup>, and Shandong Li<sup>1,\*</sup>

<sup>1</sup> College of Physics, University-Industry Joint Center for Ocean Observation and Broadband Communication, and National Demonstration Center for Experimental Applied Physics Education, Qingdao University, Qingdao 266071, China

Received: 4 January 2021

Accepted: 15 February 2021

Published online:

1 March 2021

© The Author(s), under exclusive licence to Springer Science+Business Media, LLC part of Springer Nature 2021

## ABSTRACT

With the rapid development of artificial intelligence and wearable devices, flexible magnetic sensors have attracted much attention in recent years. In this work, large self-biased 0–3 type poly(vinylidene fluoride-trifluoroethylene)/cobalt ferrite (P(VDF-TrFE)/CoFe<sub>2</sub>O<sub>4</sub>) flexible magnetoelectric (ME) composite films are proposed for the development of AC magnetic sensors. P(VDF-TrFE)/CoFe<sub>2</sub>O<sub>4</sub> composite films with CoFe<sub>2</sub>O<sub>4</sub> nanoparticle mass contents from 5 to 30% are successfully fabricated through the solution casting method. The results show that the nanoparticles are homogeneously dispersed in the P(VDF-TrFE) matrix, and the composite films have both excellent ferroelectric and ferromagnetic properties. The P(VDF-TrFE)/CoFe<sub>2</sub>O<sub>4</sub> composite films all exhibit a large ME effect. The ME coefficient reaches 47.1 mV·cm<sup>-1</sup>·Oe<sup>-1</sup> for the film with a CoFe<sub>2</sub>O<sub>4</sub> nanoparticle mass content of 20% at resonance frequency. Moreover, the composite films have a large self-biased ME effect with a maximum value of 20.4 mV·cm<sup>-1</sup>·Oe<sup>-1</sup>, which is mainly due to the high remnant magnetization of CoFe<sub>2</sub>O<sub>4</sub> nanoparticles. To evaluate the composite films for application in magnetic sensors, the response of the ME output voltage to an AC magnetic field without a bias DC magnetic field was measured. The good linear correlation coefficient, sensitivity and repeatability indicate that the proposed 0–3 type P(VDF-TrFE)/CoFe<sub>2</sub>O<sub>4</sub> composite film is a promising material for flexible AC magnetic sensors.

Handling Editor: Gregory Rutledge.

Address correspondence to E-mail: xujie@qdu.edu.cn; lishd@qdu.edu.cn

## Introduction

With the rapid development of artificial intelligence, wearable devices have attracted much attention for medical care, smart homes, communication, child-care, and so on [1–5]. Flexible sensors are widely used in wearable devices, including for sports and health monitoring [6–8]. In addition, some scholars have developed various wearable energy collectors to collect and utilize the energy signals generated by the human body [9–11]. At present, the development and application of flexible magnetic sensors are becoming increasingly extensive [12]. The application of the magnetoelectric (ME) effect in magnetic field sensors is becoming a research hot spot due to its advantages of good flexibility, high sensitivity, simple structure and low cost.

The ME effect is defined as an induced dielectric polarization in a material under an applied magnetic field or an induced magnetization under an external electric field [13]. Since the ME effect of single-phase materials was so weak and unsatisfactory for applications, researchers designed composites composed of piezoelectric and magnetostrictive materials through a strain-mediated method [14, 15]. According to the connectivity of the two components, ME composites are generally divided into 0–3, 1–3 and 2–2 types [16]. In recent years, research on 2–2 type composites has been very active due to their large ME coefficient [17]. However, the stress transfer of the epoxy between the two layers brings relaxation and loss problems [18]. The 1–3 type composites are produced by embedding magnetostrictive rods or nanowires in a piezoelectric matrix, and the greatest problem is that the rods or nanowires form electric current channels and decrease the ME effect [19]. The 0–3 type composites can solve the above problems very well because the magnetic particles can be homogeneously dispersed in and be in direct contact with the piezoelectric matrix. In particular, polymer-based 0–3 type ME composites will excel in future flexible sensors due to their excellent flexibility.

Among polymers, polyvinylidene fluoride (PVDF) has the highest piezoelectric coefficient, a low dielectric loss and a large electrical resistivity [20] and is usually applied in the piezoelectric materials of polymer-based ME composites [21]. The  $\beta$ -crystalline phase of PVDF is one of the most common polymorphic forms, which represents the polar phase and

determines the ferroelectric properties of ME composites. Many methods can be used to increase the  $\beta$ -phase content of PVDF-based ME composite films, such as heat treatment, poling and stretching [22, 23]. Poly(vinylidene fluoride-chlorotrifluoroethylene) (P(VDF-TrFE)) more easily forms an all-trans structure and has better ferroelectric properties [24]. Moreover, ferrite is a common nonmetallic magnetic material and is widely used in GMR biosensors [25], magnetic recording [26], drug delivery [27], ME composites [28] and many other fields. It was found that the type, dispersion and mass content of magnetic particles affect the ME properties of composites [29]. Martins et al. chose three different ferrite nanoparticles as fillers for 0–3 type ME composite films and found that the composite film doped with  $\text{CoFe}_2\text{O}_4$  (CFO) nanoparticles had a better ME effect than those doped with  $\text{Fe}_3\text{O}_4$  and  $\text{Zn}_{0.2}\text{Mn}_{0.8}\text{Fe}_2\text{O}_4$  nanoparticles [30]. Among them, the CFO nanoparticles have large saturation and remanent magnetization; in particular, the magnetostrictive coefficient is much larger than that of the other ferrites. Behera et al. incorporated CFO nanoparticles into PVDF and obtained an ME coefficient of  $7.5 \text{ mV}\cdot\text{cm}^{-1}\cdot\text{Oe}^{-1}$  [31]. The maximum value of the ME coefficient in the 0–3 type PVDF/CFO composite films reported in the literature is  $41 \text{ mV}\cdot\text{cm}^{-1}\cdot\text{Oe}^{-1}$  [32]. With the optimization of ME properties, 0–3 type ME composites have gradually been put into application [33]. For application in flexible magnetic sensors, a very complex problem arises. To further improve the ME coefficient, composites usually need a bias magnetic field provided by permanent magnets or electromagnets, which not only makes the sensor bulky but also brings large electromagnetic noise. The self-biased ME effect is expected to solve this problem.

In this study, we synthesized CFO nanoparticles and prepared 0–3 type P(VDF-TrFE)/CFO ME composite films. A large ME coefficient and a self-biased ME effect were found in the composite films. Then, the response of the ME output voltage to an AC magnetic field without a bias DC magnetic field was measured to evaluate the composite films for application in magnetic sensors.

## Experimental procedure

### Synthesis of $\text{CoFe}_2\text{O}_4$ nanoparticles

CFO nanoparticles were synthesized by a hydrothermal method [34].  $\text{CoCl}_2 \cdot 6\text{H}_2\text{O}$  (2.5 mmol) and  $\text{FeCl}_3 \cdot 6\text{H}_2\text{O}$  (5 mmol) were dissolved in 40 mL ethylene glycol under magnetic stirring for 1 h at room temperature. Then, with the addition of 3.6 g sodium acetate and 1 g CTAB (hexadecyl trimethyl ammonium bromide), the solution was stirred continuously for up to 4 h to mix it uniformly. The obtained brown solution was transferred to a 50 mL Teflon-lined stainless-steel autoclave, sealed and heated to 200 °C. After the reaction for 8 h, the product was collected by the use of a centrifuge and washed with ethanol and distilled water several times. Finally, CFO powder was obtained by drying for further experiments.

### Fabrication of P(VDF-TrFE)/ $\text{CoFe}_2\text{O}_4$ composite films

P(VDF-TrFE)/CFO composite films were prepared by the solution casting method. The CFO powder was added into 8.5 mL N,N-dimethylformamide (DMF) and sonicated for 2 h to completely disperse it. Then, 1 g P(VDF-TrFE) was dissolved in the solution and ultrasonicated and mechanically stirred for 2 and 8 h at room temperature, respectively. The aim of stirring for a long time was to obtain a sufficiently mixed colloid and avoid agglomeration of nanoparticles. After that, the above colloid was cast evenly into a mold, vacuumed for 1 h to remove air bubbles, and then dried at 60 °C for 2 h. The average thickness of the prepared P(VDF-TrFE)/CFO composite films was 50  $\mu\text{m}$ . Annealing treatment was carried out on the composite films at 140 °C for 2 h, which can increase the  $\beta$ -phase content and crystallinity and improve the density of the composite films [35]. Subsequently, the composite films were cut into squares 1.5 cm on a side, and the upper and lower surfaces were coated by conductive silver paste. Finally, polarization treatment of the samples was carried out in an oil bath at 80 °C under an electric field of 40 MV/m for 1 h. Composite films with various mass percentages of CFO nanoparticles (0, 5, 10, 15, 20, 25 and 30%) were prepared, and the samples were named P(VDF-TrFE), CF5, CF10, CF15, CF20, CF25 and CF30, respectively.

## Characterization

Crystalline structure and phase composition analysis of CFO nanoparticles and P(VDF-TrFE)/CFO composite films were carried out using an X-ray diffractometer (XRD, Rigaku D/Max, Japan). The morphology of the samples was observed using a scanning electron microscope (SEM, JSM-6390LV, Japan). The surface morphology and roughness of composite films were analyzed by an atomic force microscope (AFM, Park Systems XE7, Korea). The functional group and molecular structure characteristics of the samples were analyzed using a Fourier transform infrared spectrometer (FTIR, Thermo Scientific Nicolet iS50, USA). The ferroelectric properties and piezoelectric coefficients of the films were detected by a ferroelectric material hysteresis loop measuring instrument (ZT-4A, China) and a quasi-static piezoelectric coefficient  $d_{33}$  measuring instrument (ZJ-3, China), respectively. The magnetic properties of the samples were obtained using a SQUID magnetometer (Quantum design, USA).

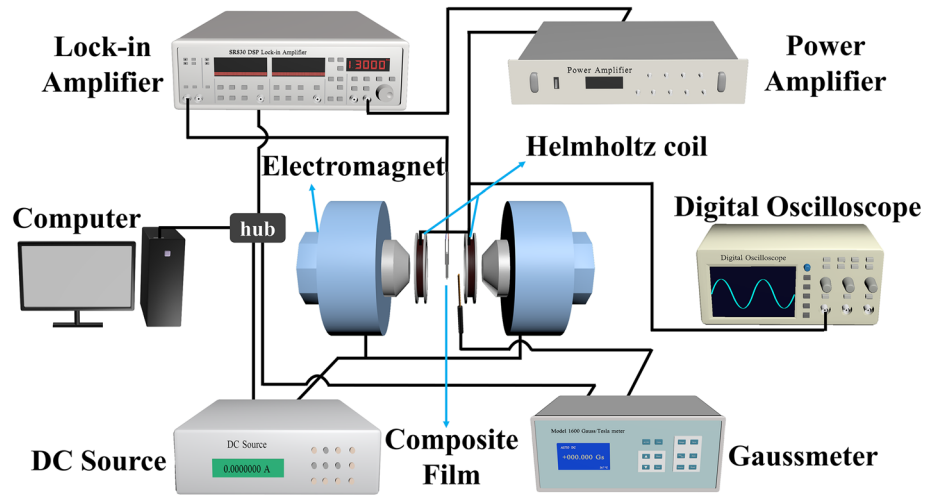
The ME output voltage of the samples was detected using the homemade measurement system of the test system. Figure 1 shows a schematic diagram. The electromagnet was driven by a DC constant current source (YL 2420, China) to supply a DC magnetic field. The sinusoidal output signal of the lock-in amplifier (Model SR830, USA) was amplified by a power amplifier (DAHA MD-150 W, China) and then connected to a Helmholtz coil to supply an AC magnetic field. The directions of the AC and DC magnetic fields were parallel. The strength was monitored in real-time by a gaussmeter (CH-1600, China). The function of the lock-in amplifier was to detect the ME voltage signal of the sample. The signal was transmitted to the computer, which recorded the data.

## Results and discussion

### Crystalline structure and phase composition analysis

As shown in Fig. 2a, the XRD pattern of the CFO nanoparticles has the typical reflections of the (111), (220), (311), (222), (400), (422), (511), (440), (531), (620), (533) and (622) planes, which are well consistent with the corresponding diffraction data of CFO particles

**Figure 1** Schematic diagram of the ME measurement system.



(PDF#22-1086) and indicate the presence of spinel-phase cobalt ferrite. The lack of additional diffraction peaks proves that pure CFO particles were synthesized successfully.

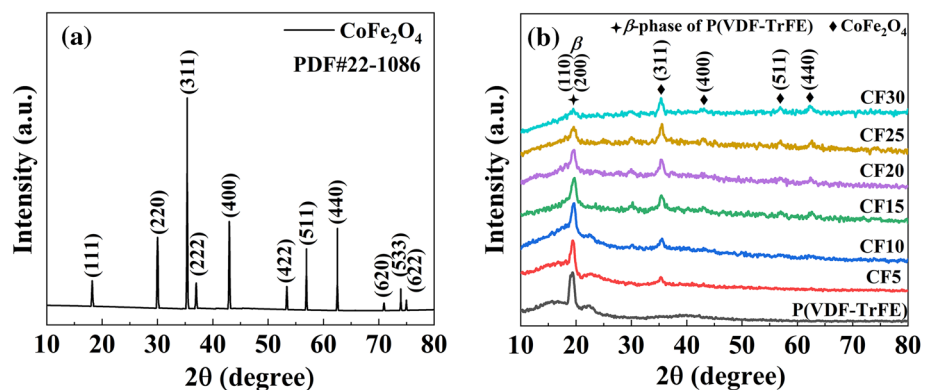
Figure 2b illustrates the X-ray diffraction patterns of the P(VDF-TrFE)/CFO composite films with different particle contents. There is an obvious peak at 20.5°, which corresponds to the  $\beta$ -crystalline phase of P(VDF-TrFE) and indicates the semicrystalline nature of the polymer [36]. The diffraction peaks of CFO nanoparticles were found in all composite samples. The presence of both CFO nanoparticles and the polymer ferroelectric  $\beta$ -phase was confirmed. With increasing CFO nanoparticle content, the intensity of the CFO nanoparticle peak increases; however, that of the P(VDF-TrFE)  $\beta$ -phase peak decreases significantly. Hence, selecting a proper CFO nanoparticle content may be important for improving the quality and performance of composite films.

### Morphological analysis

The morphology and microstructure of CFO nanoparticles are shown in Fig. 3. SEM images demonstrate that the nanoparticles have a spherical structure with a smooth surface. The corresponding histogram shows the size distribution of the particles, with an average diameter of 250 nm.

Figure 4a–f shows surface images of the composite films with different CFO nanoparticle contents. The spherical CFO nanoparticles are uniformly distributed in the P(VDF-TrFE) matrix. Significantly, interconnection and agglomeration of nanoparticles are clearly observed in samples CF25 and CF30, which will affect the ME property of the composite films. A cross-sectional SEM image of sample CF20 was obtained, as shown in Fig. 4g. The spherical CFO nanoparticles are directly and uniformly attached to P(VDF-TrFE), and no interconnection or agglomeration is found. The photograph of sample CF20 indicates excellent flexibility, as shown in Fig. 4h.

**Figure 2** XRD patterns of a CFO nanoparticles and b P(VDF-TrFE)/CFO composite films with different particle contents.



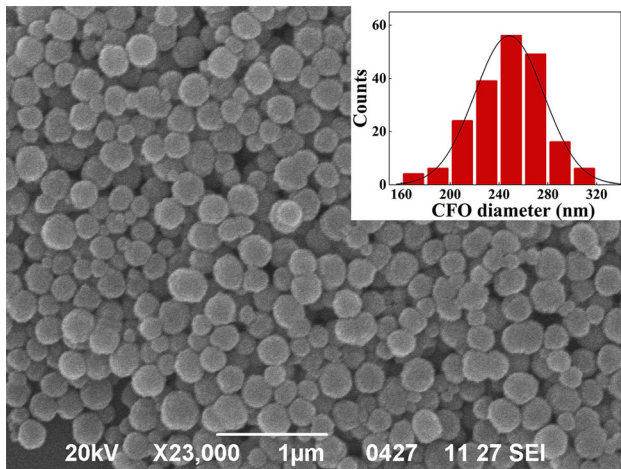


**Figure 3** SEM image of CFO nanoparticles; the inset is a histogram.

The topography of sample CF20 was analyzed with the AFM in noncontact mode and is depicted in Fig. 5. The 2D image shown in Fig. 5a confirms that there are many large spherical structures and small particles. The large spherical structures are the unique spherulitic structures of P(VDF-TrFE). The small particles are CFO nanoparticles that are distributed homogeneously in the matrix. The 3D image (Fig. 5b) shows that the roughness of the composite film is 51 nm.

## FTIR analysis

FTIR spectra of the samples are shown in Fig. 6 to research the polymorphic characteristics of P(VDF-TrFE). The characteristic peaks at 1166 and 879  $\text{cm}^{-1}$  correspond to the nonpolar  $\alpha$ -phase of P(VDF-TrFE). The peaks at 461, 504, 840, 1120, 1291, 1400 and 1431  $\text{cm}^{-1}$  belong to the stretching vibration of the P(VDF-TrFE) polar  $\beta$ -phase. The excellent ferroelectric and piezoelectric properties of the films are provided by the polar  $\beta$ -phase. The content percentage of the  $\beta$ -phase in the P(VDF-TrFE) films can be calculated by the following equation [37]:

$$F(\beta) = \frac{A_{\beta}}{(K_{\beta}/K_{\alpha})A_{\alpha} + A_{\beta}} \quad (1)$$

where  $A_{\alpha}$  and  $A_{\beta}$  are the absorbance intensities at wavenumbers 760 and 838  $\text{cm}^{-1}$ , and  $K_{\alpha}$  and  $K_{\beta}$  are the absorption coefficients at the corresponding wavenumbers, whose values are  $6.1 \times 10^{-4}$  and  $7.7 \times 10^{-4} \text{ cm}^2/\text{mol}$ , respectively. The  $\beta$ -phase contents of the samples are 80.1%, 91.6%, 97.1%, 93.4%, 90.2%, 73.4% and 69.5% for pure P(VDF-TrFE), CF5, CF10, CF15, CF20, CF25 and CF30, respectively. Interestingly, with increasing CFO nanoparticle content, the  $\beta$ -phase content first increases and then decreases. The maximum value reaches 97.1% in the CF10 sample. Initially, the addition of a small amount of nanoparticles helps induce the electroactive  $\beta$ -

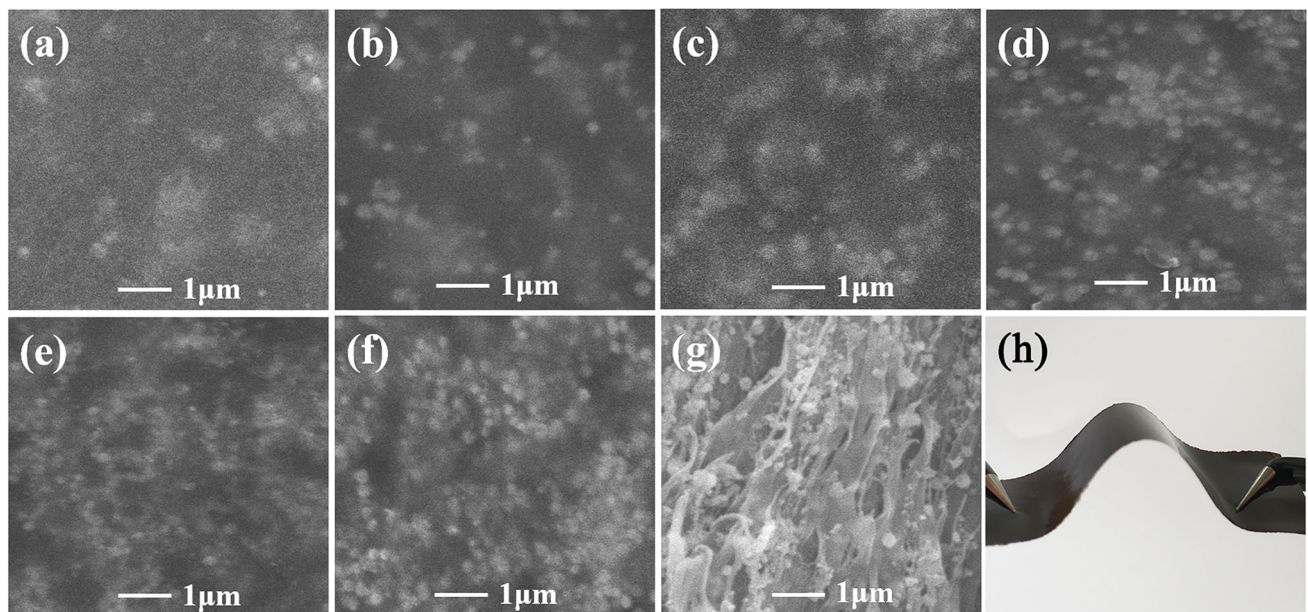


**Figure 4** Surface SEM images of P(VDF-TrFE)/CFO composite films with different CFO contents: **a** CF5, **b** CF10, **c** CF15, **d** CF20, **e** CF25 and **f** CF30; **g** cross-sectional SEM image of sample CF20; **h** photograph of sample CF20.

**Figure 5** a 2D and b 3D AFM images of sample CF20.

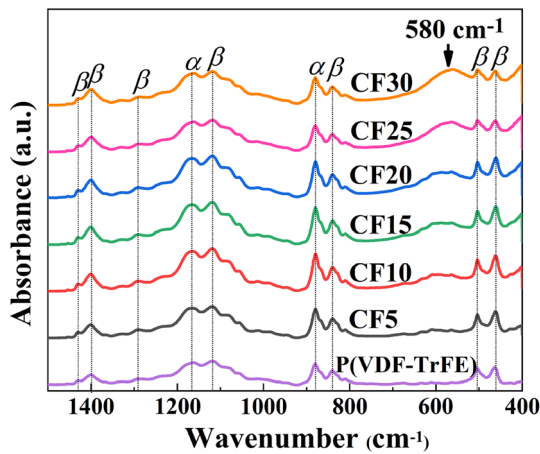
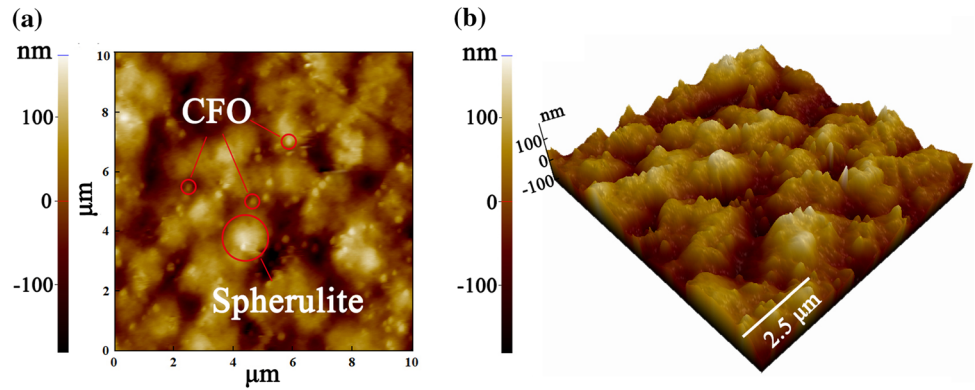


**Figure 6** FTIR spectra of the pure P(VDF-TrFE) film and P(VDF-TrFE)/CFO composite films with different CFO contents.

phase in the polymer matrix because CFO nanoparticles as nucleating agents and the strong electrostatic interaction between the nanoparticles and polymer in the interface area can improve the electrical properties of the composite films. However, with a further increase in CFO content, more nucleating centers will lead to more crystal defects, and the  $\beta$ -phase content will begin to decrease [38–42]. Moreover, there is a broad absorption peak near  $580\text{ cm}^{-1}$ , corresponding to the characteristic peak of spinel ferrite [43]. It can be found that with increasing CFO nanoparticle content, there is a significant bulge.

**Polarization treatment**

To obtain a better ME performance, the prepared composite films need to be polarized in an oil bath at  $80\text{ }^{\circ}\text{C}$ . A large leakage current is found for the CF25 and CF30 samples, as shown in Fig. 7, which will cause breakdown of the sample with increasing polarization voltage. This breakdown phenomenon is

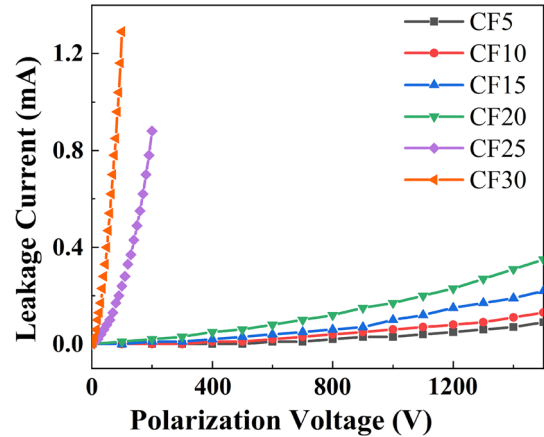


**Figure 7** Dependence of the leakage current on the polarization voltage for different samples.

mainly due to the interconnection of a large number of nanoparticles in the P(VDF-TrFE) matrix. Moreover, with increasing polarization voltage, the domain wall movement brings more interconnection of nanoparticles, which reduces the resistance and increases the leakage current of the composite films [44]. For the samples with a lower content of CFO nanoparticles, the leakage currents are small during the polarization treatments, and the samples do not break down. Therefore, samples CF5, CF10, CF15 and CF20 are selected for further discussion.

**Electrical properties**

A good piezoelectric property can significantly improve the ME effect of composite films. Figure 8 presents the dependence of the piezoelectric coefficient  $d_{33}$  on the CFO content. As the CFO content increases, the value of  $d_{33}$  first increases and then decreases, reaching a maximum value of  $25\text{ pC}\cdot\text{N}^{-1}$  when the CFO content is 10%. This changing trend of

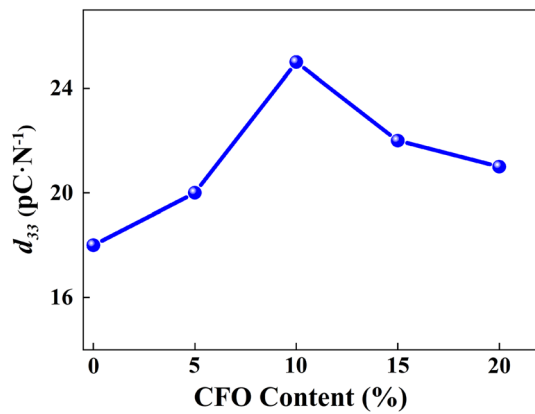


**Figure 8** Dependence of the piezoelectric coefficient on the CFO content.

$d_{33}$  agrees well with the  $\beta$ -phase content of samples previously calculated, which is mainly due to the piezoelectric property of the composites being related to the  $\beta$ -phase content.

The dependence of electric field  $E$  on electric polarization  $P$  for the samples with different CFO contents was measured under the conditions of a maximum electric field of 30 MV/m and a frequency of 1 Hz at room temperature and is shown in Fig. 9. A good signature of ferroelectric polarization is found in all samples. The maximum values of polarization  $P_{\max}$  are 5.5, 6.0, 11.3, 6.2 and 7.3 mC/m<sup>2</sup> for samples P(VDF-TrFE), CF5, CF10, CF15 and CF20, respectively. It can also be found that  $P_{\max}$  reaches the highest value in sample CF10, which also coincides with the  $\beta$ -phase content of the samples calculated from FTIR. A small amount of CFO nanoparticles can introduce extra free charges into P(VDF-TrFE)/CFO composite films, which can

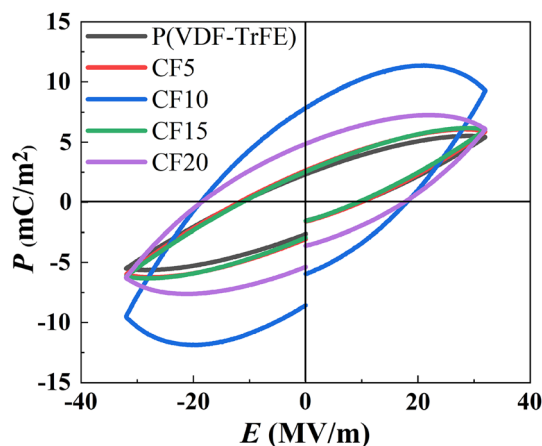


**Figure 9** Ferroelectric hysteresis loops of the pure P(VDF-TrFE) film and P(VDF-TrFE)/CFO composite films with different CFO contents.

compensate and stabilize the polarization region [45]. Moreover, CFO particles act as heterogeneous nucleation centers in the ferroelectric domain during the polarization process [30]. These reasons lead to the electric properties of the copolymer matrix being improved by doping a small amount of magnetic particles.

### Magnetic properties

In addition to the piezoelectric phase P(VDF-TrFE), the magnetic nanoparticles are another component of the ME composite films. Figure 10 shows the hysteresis loops of CFO nanoparticles and P(VDF-TrFE)/CFO composite films at room temperature.  $M_s$ ,  $M_r$  and  $H_c$  represent the saturation magnetization, residual magnetization and coercivity of the CFO nanoparticles, respectively, and their values are 76.6 emu/g, 21.1 emu/g and 1019 Oe, respectively. The  $M_s$  of the CFO nanoparticles is near the bulk magnetization value of 80.8 emu/g [46], which proves that the nanoparticles have good ferromagnetic properties. Moreover, the  $M_s$  values of composite films CF5, CF10, CF15 and CF20 are 3.8, 7.8, 11.6 and 15.0 emu/g, and the  $M_r$  values are 1.3, 2.3, 3.6 and 4.6 emu/g, respectively. With increasing CFO content, the  $M_s$  and  $M_r$  of the composite films increase, which is consistent with the values calculated theoretically according to the mass content of nanoparticles in the composite films.

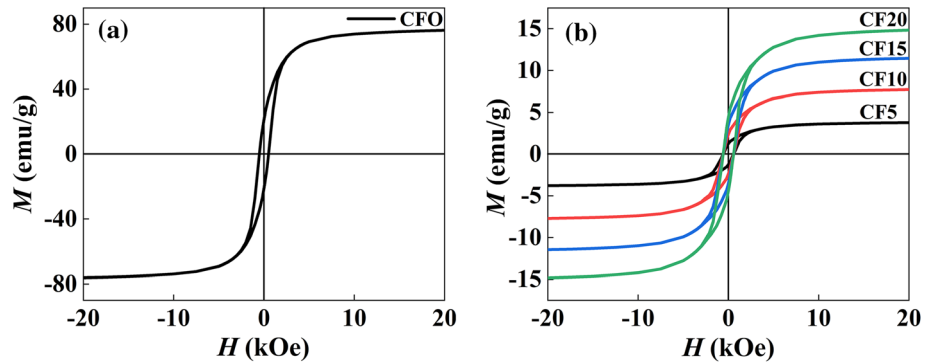
### Magnetolectric effect

The magnetolectric coupling coefficient is calculated by the following equation [47]:

$$\alpha_{\text{ME}} = \frac{\Delta V}{t \cdot H_{\text{AC}}} \quad (2)$$

where  $\Delta V$  is the measured magnetolectric output voltage,  $t$  is the thickness of the composite film, and  $H_{\text{AC}}$  is the strength of the AC magnetic field. The ME behavior of the P(VDF-TrFE)/CFO composite films was analyzed at room temperature. When composite films were operated at the resonance frequency, the ME coupling was greatly improved. To obtain the optimum resonance frequency, the response of the ME coefficient to the frequency in the range from 0.001 to 20 kHz was measured under a bias magnetic field of 2.3 kOe. From Fig. 11, one resonance peak is found at a frequency of 1.3 kHz, which corresponds

**Figure 10** Hysteresis loops of **a** CFO nanoparticles and **b** P (VDF-TrFE)/CFO composite films with different CFO contents.



to the optimum resonance frequency. Under this resonance frequency, the maximum values of  $\alpha_{ME}$  for samples CF5, CF10, CF15 and CF20 are 12.1, 24.1, 34.7 and 47.1  $\text{mV}\cdot\text{cm}^{-1}\cdot\text{Oe}^{-1}$ , respectively. The sample CF20 shows the largest ME effect. Obviously, the result is different from the analysis of  $d_{33}$ . This is because the ME effect is affected by both the piezoelectric and magnetostrictive phases.

Usually, ME films need a bias magnetic field  $H_{DC}$ . Figure 12a shows  $\alpha_{ME}$  as a function of  $H_{DC}$  under the conditions of constant frequency and  $H_{AC}$  ( $H_{AC} = 2$  Oe and  $f_{AC} = 1.3$  kHz). The  $\alpha_{ME}$  value increases with increasing DC magnetic field to 2.3 kOe (the optimum bias magnetic field), and after that, the  $\alpha_{ME}$  value decreases. The maximum  $\alpha_{ME}$  value of 47.1  $\text{mV}\cdot\text{cm}^{-1}\cdot\text{Oe}^{-1}$  is obtained in sample CF20. Table 1 summarizes the measured data of the  $\beta$ -phase content and electrical, magnetic and ME properties of the samples. Notably, the highest electrical properties are found in the CF10 sample, which corresponds to the maximum content of the  $\beta$ -phase in the composites, as discussed above. However, the highest

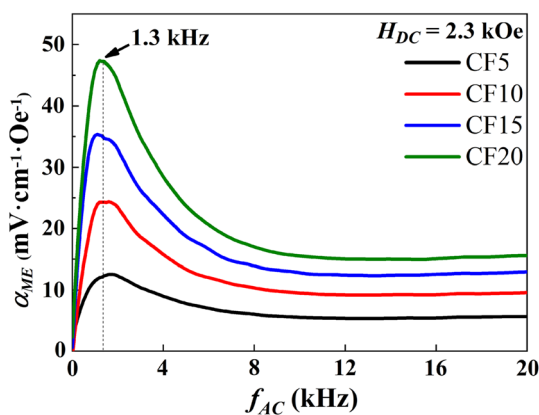


**Figure 11** Dependence of the ME coefficient on the frequency of the AC magnetic field for the P(VDF-TrFE)/CFO composite films with different CFO contents.

magnetic properties are found in the CF20 sample because the content of magnetic particles in CF20 is the highest. Since the ME effect is a comprehensive result of electric and magnetic phases and there is a more significant change for magnetic than electric properties with increasing amount of particles in the composites, the highest ME performance is obtained in the CF20 sample.

In addition, it is interesting that the samples have a large self-biased ME effect ( $\alpha_{ME,0}$ ) when  $H_{DC}$  is zero. The  $\alpha_{ME,0}$  and maximum  $\alpha_{ME}$  at 2.3 kOe of the P (VDF-TrFE)/CFO composite films with different CFO contents are shown in Fig. 12b. The value of  $\alpha_{ME,0}$  increases with increasing CFO content and reaches a maximum of 20.4  $\text{mV}\cdot\text{cm}^{-1}\cdot\text{Oe}^{-1}$  in sample CF20. As discussed in the previous section, the CFO nanoparticles prepared in this work have a high saturation magnetization near the bulk value and a large remnant magnetization. It is speculated that the high remnant magnetization of CFO nanoparticles ensures that the nanoparticles still have an obvious magnetostrictive effect under a zero DC magnetic field, which induces the self-biased ME effect of the composite films [48]. The PVDF-based ME composites reported in other literature are summarized in Table 2.

Because of the large self-biased ME effect, the composite films are expected to have technological applications. To evaluate the applicability, sample CF20 was chosen to measure the response of the ME voltage  $V_{ME}$  to AC excitation magnetic field  $H_{AC}$ . The detection was performed under a self-biased DC magnetic field and a constant frequency of the AC magnetic field ( $H_{DC} = 0$  and  $f_{AC} = 1.3$  kHz). As shown in Fig. 13a,  $V_{ME}$  varies linearly with the strength of  $H_{AC}$ , and the linear correlation coefficient and sensitivity are  $R^2 = 0.99669$  and  $S = 0.11302$  mV/Oe at the resonance frequency, respectively. The



**Figure 12** **a** Dependence of the ME coefficient on the DC bias magnetic field and **b** self-biased ME coefficient of the P (VDF-TrFE)/CFO composite films with different CFO contents.

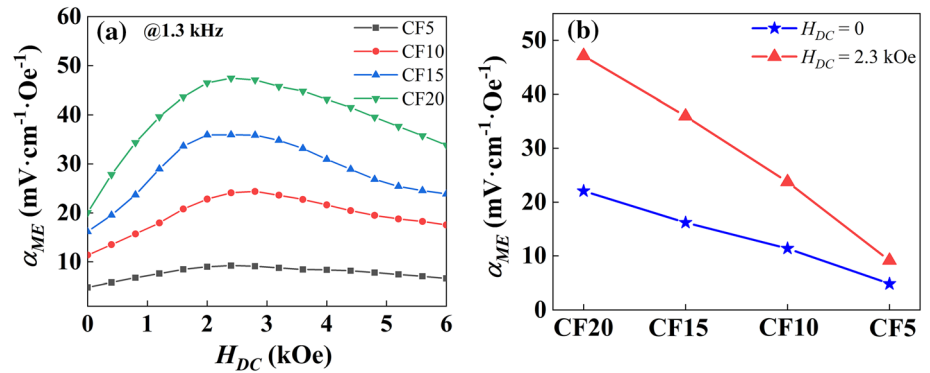


**Table 1** Summary of  $P_{max}$ ,  $d_{33}$ ,  $M_s$ ,  $M_r$ ,  $\beta$ -phase,  $\alpha_{ME}$  of all samples

	$\beta$ -phase (%)	$P_{max}$ (mC/m <sup>2</sup> )	$d_{33}$ (pC·N <sup>-1</sup> )	$M_s$ (emu/g)	$M_r$ (emu/g)	$\alpha_{ME}$ ( $\text{mV}\cdot\text{cm}^{-1}\cdot\text{Oe}^{-1}$ )	$\alpha_{ME,0}$ ( $\text{mV}\cdot\text{cm}^{-1}\cdot\text{Oe}^{-1}$ )
P(VDF-TrFE)	80.1	5.5	18	–	–	–	–
CF5	91.6	6.0	20	3.8	1.3	12.1	4.8
CF10	97.1	11.3	25	7.8	2.3	24.1	11.4
CF15	93.4	6.2	22	11.6	3.6	34.7	16.2
CF20	90.2	7.3	21	15.0	4.6	47.1	22.0

excellent linearity ensures that the sample is suitable for the development of AC magnetic field sensors. To explore the difference between the experimental data and linear fit, the deviation (D) was calculated with the following formula:

$$D = \frac{V_{fit} - V_{out}}{V_{fit}} \times 100\% \quad (3)$$

where  $V_{out}$  and  $V_{fit}$  are the experimental and fitted data, respectively. The maximum error is 0.039 mV, which is in an acceptable range. The large deviation under the low AC magnetic field of 1 Oe may be caused by the strong signal interference under this

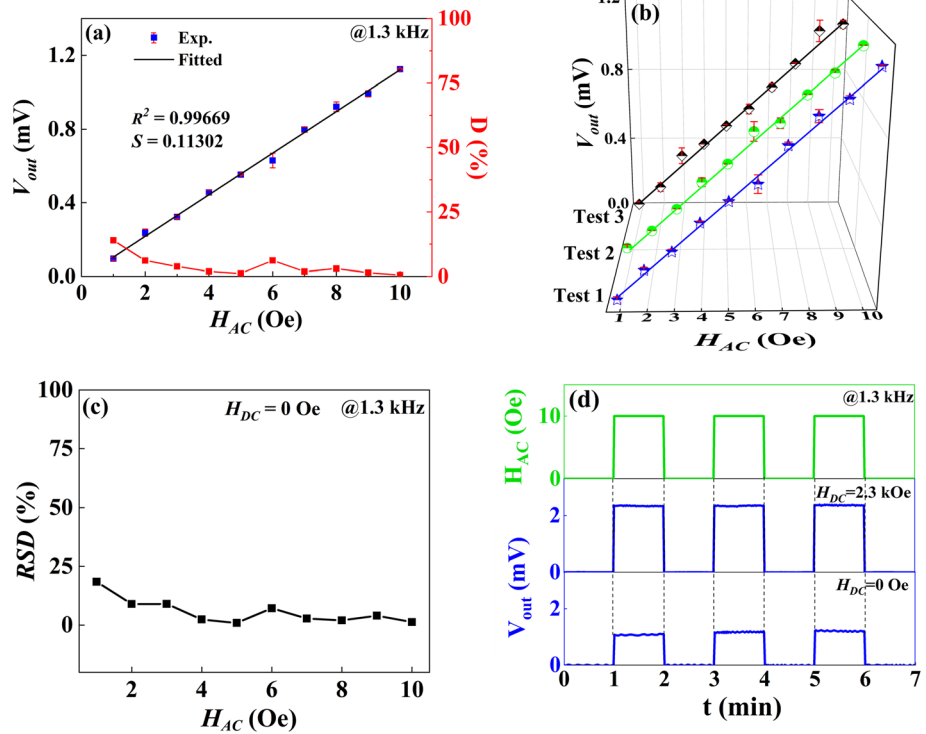
low magnetic field. Under other AC magnetic field strengths, the deviation is stable within 6%. The deviation is also within the acceptable range.

Then, we repeated the detection three times, and the results are shown in Fig. 13b. The error between all experimental and fitted data is within 0.047 mV, which indicates that the composite films can be reused and that the detection results maintain good consistency. The relative standard deviations (RSDs) were calculated by the following equation:

**Table 2** Comparison of  $\alpha_{ME}$  with other literature

Sample	$\beta$ -phase content	Particle size (nm)	$\alpha_{ME}$ ( $\text{mV}\cdot\text{cm}^{-1}\cdot\text{Oe}^{-1}$ )	Ref
PVDF/CFO	78.7%	20	–	[22]
P(VDF-HFP)/CFO	50%	31–43	–	[23]
P(VDF-TrFE)/CFO	–	80–100	32	[29]
PVDF/CFO	–	10	7.5	[31]
P(VDF-TrFE)/CFO	–	35–55	41	[32]
PVDF/La <sub>2</sub> NiMnO <sub>6</sub>	37%	200 ~ 300	9.6	[36]
PVDF/BTO/CFO	–	–	26	[49]
PVDF/CFO	88%	–	–	[50]
PVDF/ZFO	92%	58	–	[51]
P(VDF-TrFE)/CFO	97.1%	250	47.1	This work

**Figure 13** **a** ME voltage of sample CF20 in response to the strength of the AC magnetic field at a resonance frequency of 1.3 kHz. **b** Comparison of three detection results of the ME voltage of sample CF20 in response to the strength of the AC magnetic field at a resonance frequency of 1.3 kHz. **c** Relative standard deviation calculated from the data of the three detections. **d** ME voltage of sample CF20 in response to changes in the AC magnetic field between “on” and “off” under the zero DC magnetic field and optimal bias field of 2.3 kOe.



$$RSD = \left( \sqrt{\frac{\sum_{i=1}^n (V_{ME,i} - \overline{V_{ME}})^2}{n - 1}} / \overline{V_{ME}} \right) \times 100\% \tag{4}$$

where  $V_{ME,i}$ ,  $\overline{V_{ME}}$  and  $n$  refer to the  $i$ -th measured voltage value, average voltage value and number of measurements, respectively. Figure 13c shows the dependence of RSD on the strength of the AC magnetic field. When the AC magnetic field is 1 Oe, RSD has a maximum value of 18%. With increasing AC magnetic field, the value of RSD decreases rapidly below 10% and then gradually levels off. The large RSD for the small magnetic field is mainly due to the stronger signal interference.

Figure 13d shows the  $V_{ME}$  of sample CF20 in response to changes in the AC magnetic field. As the signal of the AC magnetic field changes between “on” and “off,”  $V_{ME}$  can be responsive in time and remain stable for both the zero DC magnetic field and optimal bias field of 2.3 kOe at 1.3 kHz. The results indicate that the 0–3 PVDF/CFO composite film is a promising flexible magnetic sensor material.

### Conclusions

Spherical CFO nanoparticles were synthesized and used as fillers to prepare 0–3 type P(VDF-TrFE)/CFO ME composite films with different CFO contents. The structural, functional, piezoelectric, ferroelectric and magnetic behaviors of the composite films were studied. Through characterization, we found that the CFO nanoparticles are well dispersed in the P(VDF-TrFE) matrix. The composite films show both excellent ferroelectric and ferromagnetic properties. In addition, the ME effect is observed for the composite films with CFO contents under 20% due to the breakdown of samples CF25 and CF30. The largest ME coefficient of  $47.1 \text{ mV}\cdot\text{cm}^{-1}\cdot\text{Oe}^{-1}$  is found in sample CF20 at the resonance frequency. Moreover, sample CF20 has a large self-biased ME coupling coefficient of  $20.4 \text{ mV}\cdot\text{cm}^{-1}\cdot\text{Oe}^{-1}$ . Thus, the composite films are expected to have technological applications in magnetic field sensors. Finally, sample CF20 was chosen to measure the response of  $V_{ME}$  to  $H_{AC}$ .  $V_{ME}$  can be responsive in time and remain stable with changes in  $H_{AC}$  for both a zero DC magnetic field and the optimal bias field of 2.3 kOe. Good linear correlation coefficient, sensitivity and RSD were found, indicating that the 0–3 PVDF/CFO composite film is a promising flexible magnetic sensor material.

## Acknowledgements

This work was financially supported by the National Natural Science Foundation of China (NNSFC) with Grant Nos. 11604172, 11674187, and 51871127.

## Compliance with ethical standards

**Conflict of interest** The authors declare that they have no conflicts of interest.

## References

- [1] Rogers JA (2017) Wearable electronics nanomesh on-skin electronics. *Nat Nanotechnol* 12(9):839–840. <https://doi.org/10.1038/nnano.2017.150>
- [2] Hatamie A, Angizi S, Kumar S, Pandey CM, Simchi A, Willander M, Malhotra BD (2020) Review-textile based chemical and physical sensors for healthcare monitoring. *J Electrochem Soc* 167(3):14. <https://doi.org/10.1149/1945-7111/ab6827>
- [3] Mukhopadhyay SC (2015) Wearable sensors for human activity monitoring: a review. *IEEE Sens J* 15(3):1321–1330. <https://doi.org/10.1109/JSEN.2014.2370945>
- [4] Muzammal M, Talat R, Sodhro AH, Pirbhulal S (2020) A multi-sensor data fusion enabled ensemble approach for medical data from body sensor networks. *Inf Fusion* 53:155–164. <https://doi.org/10.1016/j.inffus.2019.06.021>
- [5] Yang JC, Mun J, Kwon SY, Park S, Bao ZN, Park S (2019) Electronic skin: recent progress and future prospects for skin-attachable devices for health monitoring, robotics, and prosthetics. *Adv Mater* 31(48):50. <https://doi.org/10.1002/adma.201904765>
- [6] Shin KY, Lee JS, Jang J (2016) Highly sensitive, wearable and wireless pressure sensor using free-standing ZnO nanoneedle/PVDF hybrid thin film for heart rate monitoring. *Nano Energy* 22:95–104. <https://doi.org/10.1016/j.nanoen.2016.02.012>
- [7] Choi S, Jiang ZW (2006) A novel wearable sensor device with conductive fabric and PVDF film for monitoring cardiorespiratory signals. *Sens Actuator A Phys* 128(2):317–326. <https://doi.org/10.1016/j.sna.2006.02.012>
- [8] Kweon OY, Lee SJ, Oh JH (2018) Wearable high-performance pressure sensors based on three-dimensional electrospun conductive nanofibers. *NPG Asia Mater* 10:12. <https://doi.org/10.1038/s41427-018-0041-6>
- [9] Xue H, Yang Q, Wang DY, Luo WJ, Wang WQ, Lin MS, Liang DL, Luo QM (2017) A wearable pyroelectric nanogenerator and self-powered breathing sensor. *Nano Energy* 38:147–154. <https://doi.org/10.1016/j.nanoen.2017.05.056>
- [10] Huang T, Wang C, Yu H, Wang HZ, Zhang QH, Zhu MF (2015) Human walking-driven wearable all-fiber triboelectric nanogenerator containing electrospun polyvinylidene fluoride piezoelectric nanofibers. *Nano Energy* 14:226–235. <https://doi.org/10.1016/j.nanoen.2015.01.038>
- [11] Mokhtari F, Shamshirsaz M, Latifi M, Foroughi J (2020) Nanofibers-based piezoelectric energy harvester for self-powered wearable technologies. *Polymers*. <https://doi.org/10.3390/polym12112697>
- [12] Wang ZG, Wang XJ, Li MH, Gao Y, Hu ZQ, Nan TX, Liang XF, Chen HH, Yang J, Cash S, Sun NX (2016) Highly sensitive flexible magnetic sensor based on anisotropic magnetoresistance effect. *Adv Mater* 28(42):9370. <https://doi.org/10.1002/adma.201602910>
- [13] Zhai J, Cai N, Shi Z, Lin Y, Nan CW (2004) Magnetic-dielectric properties of NiFe<sub>2</sub>O<sub>4</sub>/PZT particulate composites. *J Phys D Appl Phys* 37(6):823–823. <https://doi.org/10.1088/0022-3727/37/6/002>
- [14] Fiebig M (2005) Revival of the magnetoelectric effect. *J Phys D Appl Phys* 38(8):R123–R152. <https://doi.org/10.1002/chin.200533283>
- [15] Vaz CAF, Hoffman J, Ahn CH, Ramesh R (2010) Magneto-electric coupling effects in multiferroic complex oxide composite structures. *Adv Mater* 22(26–27):2900–2918. <https://doi.org/10.1002/adma.200904326>
- [16] Nan CW, Bichurin MI, Dong SX, Viehland D, Srinivasan G (2008) Multiferroic magnetoelectric composites: Historical perspective, status, and future directions. *J Appl Phys* 103(3):35. <https://doi.org/10.1063/1.2836410>
- [17] Shi M, Zuo RZ, Xu YD, Wang L, Gu C, Su HL, Zhong JG, Yu GY (2014) Preparation and multiferroic properties of 2–2 type CoFe<sub>2</sub>O<sub>4</sub>/Pb(Zr, Ti)O<sub>3</sub> composite films with different structures. *Ceram Int* 40(7):9249–9256. <https://doi.org/10.1016/j.ceramint.2014.01.146>
- [18] Martins P, Moya X, Phillips LC, Kar-Narayan S, Mathur ND, Lancesos-Mendez S (2011) Linear anhysteretic direct magnetoelectric effect in Ni<sub>0.5</sub>Zn<sub>0.5</sub>Fe<sub>2</sub>O<sub>4</sub>/poly(vinylidene fluoride-trifluoroethylene) 0–3 nanocomposites. *J Phys D Appl Phys*. <https://doi.org/10.1088/0022-3727/44/48/482001>
- [19] Bai YL, Jiang N, Zhao SF (2018) Giant magnetoelectric effects in pseudo 1–3 heterostructure films with FeGa nanocluster-assembled micron-scale discs embedded into Bi<sub>5</sub>Ti<sub>3</sub>FeO<sub>15</sub> matrices. *Nanoscale* 10(21):9816–9821. <https://doi.org/10.1039/C7NR09652F>
- [20] Chakraborty S, Mandal SK, Saha B (2019) Magneto-optic and magneto-electric effects in poly(vinylidene fluoride)-Zn<sub>0.2</sub>Co<sub>0.8</sub>Fe<sub>2</sub>O<sub>4</sub> nanocomposite organic flexible film. *Ceram Int* 45(12):14851–14858. <https://doi.org/10.1016/j.ceramint.2019.04.216>

- [21] Martins P, Larrea A, Goncalves R, Botelho G, Ramana EV, Mendiratta SK, Sebastian V, Lanceros-Mendez S (2015) Novel anisotropic magnetoelectric effect on delta-FeO(OH)/P(VDF-TrFE) multiferroic composites. *ACS Appl Mater Interfaces* 7(21):11224–11229. <https://doi.org/10.1021/acami.5b01196>
- [22] Choi MH, Yang SC (2018) CoFe<sub>2</sub>O<sub>4</sub> nanofiller effect on beta-phase formation of PVDF matrix for polymer-based magnetoelectric composites. *Mater Lett* 223:73–77. <https://doi.org/10.1016/j.matlet.2018.04.024>
- [23] Divya S, Hemalatha J (2017) Study on the enhancement of ferroelectric beta phase in P(VDF-HFP) films under heating and poling conditions. *Eur Polym J* 88:136–147. <https://doi.org/10.1016/j.eurpolymj.2017.01.016>
- [24] Martins P, Lopes AC, Lanceros-Mendez S (2014) Electroactive phases of poly(vinylidene fluoride): determination, processing and applications. *Prog Polym Sci* 39(4):683–706. <https://doi.org/10.1016/j.progpolymsci.2013.07.006>
- [25] Guan MJ, Mu XJ, Zhang H, Zhang Y, Xu J, Li Q, Wang X, Cao DR, Li SD (2019) Spindle-like Fe<sub>3</sub>O<sub>4</sub> nanoparticles for improving sensitivity and repeatability of giant magnetoresistance biosensors. *J Appl Phys* 126(6):6. <https://doi.org/10.1063/1.5096345>
- [26] Jia Z, Misra RDK (2011) Micromagnetic modelling of new generation of FePt and FeRh nanostructures for heat assisted magnetic recording. *Mater Technol* 26(4):200–205. <https://doi.org/10.1179/175355511X13109965351112>
- [27] Rana S, Gallo A, Srivastava RS, Misra RDK (2007) On the suitability of nanocrystalline ferrites as a magnetic carrier for drug delivery: functionalization, conjugation and drug release kinetics. *Acta Biomater* 3(2):233–242. <https://doi.org/10.1016/j.actbio.2006.10.006>
- [28] Adhlakha N, Yadav KL, Singh R (2014) Effect of BaTiO<sub>3</sub> addition on structural, multiferroic and magneto-dielectric properties of 0.3CoFe<sub>2</sub>O<sub>4</sub>-0.7BiFeO<sub>3</sub> ceramics. *Smart Mater Struct* 23(10):16. <https://doi.org/10.1088/0964-1726/23/10/105024>
- [29] Zhang JX, Dai JY, So LC, Sun CL, Lo CY, Or SW, Chan HLW (2009) The effect of magnetic nanoparticles on the morphology, ferroelectric, and magnetoelectric behaviors of CFO/P(VDF-TrFE) 0–3 nanocomposites. *J Appl Phys* 105(5):6. <https://doi.org/10.1063/1.3078111>
- [30] Martins P, Lasheras A, Gutierrez J, Barandiaran JM, Orue I, Lanceros-Mendez S (2011) Optimizing piezoelectric and magnetoelectric responses on CoFe<sub>2</sub>O<sub>4</sub>/P(VDF-TrFE) nanocomposites. *J Phys D Appl Phys*. <https://doi.org/10.1088/0022-3727/44/49/495303>
- [31] Behera C, Choudhary RNP, Das PR (2017) Development of Multiferroism in PVDF with CoFe<sub>2</sub>O<sub>4</sub> Nanoparticles. *J Polym Res* 24(4):13. <https://doi.org/10.1007/s10965-017-1208-5>
- [32] Martins P, Goncalves R, Lanceros-Mendez S, Lasheras A, Gutierrez J, Barandiaran JM (2014) Effect of filler dispersion and dispersion method on the piezoelectric and magnetoelectric response of CoFe<sub>2</sub>O<sub>4</sub>/P(VDF-TrFE) nanocomposites. *Appl Surf Sci* 313:215–219. <https://doi.org/10.1016/j.apsusc.2014.05.187>
- [33] Zhang JM, He XZ, Chen XY, Wu YJ, Dong LQ, Cheng K, Lin J, Wang HM, Weng WJ (2020) Enhancing osteogenic differentiation of BMSCs on high magnetoelectric response films. *Mater Sci Eng C Mater Biol Appl* 113:10. <https://doi.org/10.1016/j.msec.2020.110970>
- [34] Deng H, Li XL, Peng Q, Wang X, Chen JP, Li YD (2005) Monodisperse magnetic single-crystal ferrite microspheres. *Angew Chem Int Edit* 44(18):2782–2785. <https://doi.org/10.1002/anie.200462551>
- [35] Zhou Z, Zhang Z, Zhang QL, Yang H, Zhu YL, Wang YY, Chen L (2020) Controllable core-shell BaTiO<sub>3</sub>@carbon nanoparticle-enabled P(VDF-TrFE) composites: a cost-effective approach to high-performance piezoelectric nanogenerators. *ACS Appl Mater Interfaces* 12(1):1567–1576. <https://doi.org/10.1021/acami.9b18780>
- [36] Tiwary S, Kuila S, Sahoo MR, Barik A, Ghosh IR, Babu PD, Deshpande U, Vishwakarma PN (2020) La<sub>2</sub>NiMnO<sub>6</sub>/poly(vinylidene fluoride) nanocomposites with enhanced magnetoelectric voltage. *J Appl Phys* 127(13):9. <https://doi.org/10.1063/1.5140710>
- [37] Gregorio R, Cestari M (1994) Effect of crystallization temperature on the crystalline phase content and morphology of poly(vinylidene fluoride). *J Polym Sci Pt B Polym Phys* 32(5):859–870. <https://doi.org/10.1002/polb.1994.090320509>
- [38] Prabhakaran T, Hemalatha J (2016) Magnetoelectric investigations on poly(vinylidene fluoride)/NiFe<sub>2</sub>O<sub>4</sub> flexible films fabricated through a solution casting method. *RSC Adv* 6(90):86880–86888. <https://doi.org/10.1039/C6RA18032A>
- [39] Martins P, Costa CM, Lanceros-Mendez S (2011) Nucleation of electroactive beta-phase poly(vinylidene fluoride) with CoFe<sub>2</sub>O<sub>4</sub> and NiFe<sub>2</sub>O<sub>4</sub> nanofillers: a new method for the preparation of multiferroic nanocomposites. *Appl Phys A Mater Sci Process* 103(1):233–237. <https://doi.org/10.1007/s00339-010-6003-7>
- [40] Liu X, Liu S, Han M-G, Zhao L, Deng H, Li J, Zhu Y, Krusin-Elbaum L, O'Brien S (2013) Magnetoelectricity in CoFe<sub>2</sub>O<sub>4</sub> nanocrystal-P(VDF-HFP) thin films. *Nanoscale Res Lett* 8(1):374. <https://doi.org/10.1186/1556-276X-8-374>
- [41] Goncalves R, Martins P, Correia DM, Sencadas V, Vilas JL, Leon LM, Botelho G, Lanceros-Mendez S (2015) Development of magnetoelectric CoFe<sub>2</sub>O<sub>4</sub>/poly(vinylidene

- fluoride) microspheres. *RSC Adv* 5(45):35852–35857. <https://doi.org/10.1039/c5ra04409j>
- [42] Martins P, Kolen'ko YV, Rivas J, Lanceros-Mendez S (2015) Tailored magnetic and magnetoelectric responses of polymer-based composites. *ACS Appl Mater Interfaces* 7(27):15017–15022. <https://doi.org/10.1021/acsami.5b04102>
- [43] Waldron RD (1955) Infrared spectra of ferrites. *Phys Rev* 99(6):1727–1735. <https://doi.org/10.1103/physrev.99.1727>
- [44] Qi B, Zhang YD, Yao TP (2020) magnetic field sensing based on magnetoelectric coupling of ampere force effect with piezoelectric effect in Silver/Poly(Vinylidene Fluoride)/Silver Laminated Composite. *IEEE Access* 8:68049–68056. <https://doi.org/10.1109/ACCESS.2020.2986174>
- [45] Kusuma DY, Nguyen CA, Lee PS (2010) Enhanced ferroelectric switching characteristics of P(VDF-TrFE) for organic memory devices. *J Phys Chem B* 114(42):13289–13293. <https://doi.org/10.1021/jp105249f>
- [46] Prabhakaran T, Hemalatha J (2016) Combustion synthesis and characterization of cobalt ferrite nanoparticles. *Ceram Int* 42(12):14113–14120. <https://doi.org/10.1016/j.ceramint.2016.06.025>
- [47] Martins P, Nunes JS, Oliveira J, Perinka N, Lanceros-Mendez S (2020) Spray-printed magnetoelectric multifunctional composites. *Compos Pt B Eng* 187:6. <https://doi.org/10.1016/j.compositesb.2020.107829>
- [48] Jing WQ, Fang F (2017) A flexible multiferroic composite with high self-biased magnetoelectric coupling. *Compos Sci Technol* 153:145–150. <https://doi.org/10.1016/j.compscitech.2017.10.010>
- [49] Gupta A, Chatterjee R (2009) Magnetic, dielectric, magnetoelectric, and microstructural studies demonstrating improved magnetoelectric sensitivity in three-phase BaTiO<sub>3</sub>-CoFe<sub>2</sub>O<sub>4</sub>-poly(vinylidene-fluoride) composite. *J Appl Phys.* <https://doi.org/10.1063/1.3181061>
- [50] Durgaprasad P, Hemalatha J (2018) Magnetoelectric investigations on poly (vinylidene fluoride)/CoFe<sub>2</sub>O<sub>4</sub> flexible electrospun membranes. *J Magn Magn Mater* 448:94–99. <https://doi.org/10.1016/j.jmmm.2017.08.063>
- [51] Prasad PD, Hemalatha J (2019) Dielectric and energy storage density studies in electrospun fiber mats of polyvinylidene fluoride (PVDF)/zinc ferrite (ZnFe<sub>2</sub>O<sub>4</sub>) multiferroic composite. *Phys B* 573:1–6. <https://doi.org/10.1016/j.physb.2019.08.023>

**Publisher's Note** Springer Nature remains neutral with regard to jurisdictional claims in published maps and institutional affiliations.